ADVANCED HEALTHCARE MATERIALS
www.advhealthmat.de

Microfabricated Gaps Reveal the Effect of Geometrical Control in Wound Healing

Min Bao, Jing Xie, Aigars Piruska, Xinyu Hu, and Wilhelm T. S. Huck**

The geometry (size and shape) of gaps is a key determinant in controlling gap closure during wound healing. However, conventional methods for creating gaps result in un-defined geometries and poorly characterized conditions (cell death factors and cell debris), which can influence the gap closure process. To overcome these limitations, a novel method to create well-defined geometrical gaps is developed. First, smooth muscle cells (SMCs) are seeded in variously shaped micro-containers made out of hyaluronic acid hydrogels. Cell proliferation and cell tension induce fibrous collagen production by SMCs predominantly around the edges of the micro-containers. Upon removal of SMCs, the selectively deposited collagen results in micro-containers with cell-adhesive regions along the edges and walls. Fibroblasts are seeded in these micro-containers, and upon attaching and spreading, they naturally form gaps with different geometries. The rapid proliferation of fibroblasts from the edge results in filling and closure of the gaps. It is demonstrated that gap closure rate as well as closure mechanism is strongly influenced by geometrical features, which points to an important role for cellular tension and cell proliferation in gap closure.

1. Introduction

The closure of gaps in tissues is of great importance in various biological processes,[1,2] as gaps with different geometries may naturally occur during morphogenesis, organ development, and apoptotic cells extrusion.[3,4] In adults, gaps can result from injuries and during wound healing.[5,6] In all these situations, gaps need to be closed properly to maintain normal development and re-build tissue function.

A number of in vitro models that mimic tissue gaps have been proposed to study the mechanism of gap closure. Two distinct mechanisms have been studied extensively, known as "purse-string" and "cell crawling,"[2,3,7–9] while Sakar et al. reported the collective cell migration coupled with tissues deformations and matrix assembly during stromal gap closure.[10] At the early stages of gap closure, cells, both proximal and distal to the gap, can migrate to close the gap through "crawling" by forming lamellipodial protrusions,[9,11–14] which are characterized by a rough edge.[15] Cell crawling with lamellipodial protrusion can be observed in cell sheets on flat substrates with continuous extracellular matrix (ECM) coating.[9,16,17] At later stages of gap closure, cells around the gap can collectively assemble a multi-cellular actomyosin bundle, known as a "purse-string," which induces the edge of gap to be more circular with a smooth edge.[18,19] Such mechanisms can be observed on an intact monolayer that is damaged by scratching with a pipette tip or razor blade;[14,20] this mechanism would also close gaps over non-adherent substrates.

A variety of factors have been proposed that regulate the gap closure rate, including substrate adhesion, stiffness, topography, and gap geometry.[2,3,21–24] Among those factors, the geometry of the gap has been shown to be a key determinant in controlling gap closure and cell migration. For example, the geometry of the gap edge has been reported to promote cellular traction forces in the regions of higher curvature, and thus direct outward cell migration.[2,21] A convex gap edge (positive curvature) has been associated with lamellipodial protrusion formation and cell crawling-based closure, whereas concave gap edges (negative curvature) favor actin cable assembly and purse-string-based closure.[2] Geometrical confinement on flat substrates can also affect the speed of collective migration. Madin-Darby Canine Kidney (MDCK) cells confined on strip patterns of different widths showed an increase in the speed of collective migration on more narrow strips.[25] However, it should be noted that the methods used for creating gaps in those studies were mainly based on scratch-wounding,[2,8,9,16,22,23,26] in which a sheet of epithelial or fibroblast cells is mechanically removed by a razor blade, microdissection knife, or pipette tips.[26] Some studies reported using laser ablation [12] or electrode [27] to create small wounds, in which cells are destroyed by a voltage or laser pulse. However, it is impossible to standardize those techniques, as the final geometry and size of the gap depend either on the velocity and shape

Dr. M. Bao, Dr. J. Xie, Dr. A. Piruska, X. Hu, Prof. W. T. S. Huck
Institute for Molecules and Materials
Radboud University
Heyendaalseweg 135, Nijmegen 6525 AJ, The Netherlands
E-mail: m.bao@science.ru.nl; w.huck@science.ru.nl
Dr. M. Bao
Division of Biology and Biological Engineering
California Institute of Technology
1200 E. California Boulevard Pasadena, CA 91125, USA
The ORCID identification number(s) for the author(s) of this article can be found under https://doi.org/10.1002/adhm.202000630

DOI: 10.1002/adhm.202000630

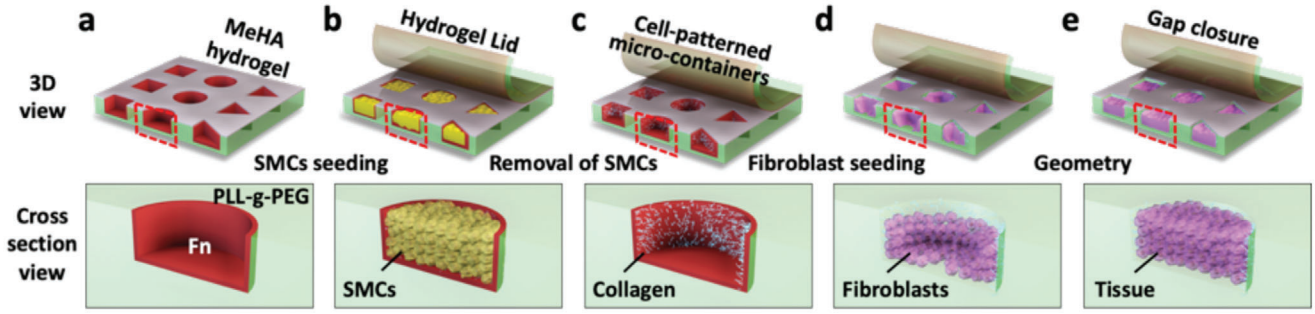

Figure 1. Schematic overview of the gap formation strategy. a) Micro-containers with different geometries were formed by photopolymerizing methacrylated hyaluronic acid (MeHA) against a silicon master with different patterns. The surface of the MeHA hydrogel was coated with poly(L-lysine)-graft-poly(ethylene glycol) (PLL-g-PEG) using a wet-stamping technique to prevent cells from adhering to the top surface; the inside of micro-containers was functionalized by fibronectin to promote cell spreading. b) Smooth muscle cells (SMCs) were seeded inside the micro-containers, and covered with a hydrogel lid. c) After culturing, SMCs and fibronectin were removed by EDTA and Triton-X100 treatment, followed by gently washing with PBS. d,e) Fibroblasts were seeded in micro-containers to investigate the effect of geometry on gap closure mechanism.

of the scratching utensil or on the laser and electricity power. In addition, a complex and poorly characterized mixture of signaling molecules, death factors, and cell debris can be released from the process of wound production that influence the efficiency of gap closure.[3]

Furthermore, we note that porous scaffolds are frequently used in tissue engineering studies,[28] and the network structure of pores guides and promotes the formation of new tissue.[29] It is important to develop a better understanding of how the geometry of pores influences pore filling and tissue growth.

Thus, there is a need for simple methods that produce "naturally formed" gaps with well-defined geometrical conditions. Here, we show a route to produce such gaps and study how geometry influences and determines cell proliferation, actomyosin activity, and the dynamics of gap closure. We demonstrate that local growth rates are strongly influenced by the geometrical features, which can be explained by the generation of mechanical forces in confined geometries and locally enhanced proliferation rates within the tissue.

2. Results and Discussions

2.1. Microfabrication of Undamaged Gaps with Well-Defined Geometries

Conventional methods of coating micro-containers with collagen monomer resulted in homogenous distribution of cells, as the collagen covered entire surfaces of the micro-containers. We therefore sought a method to differentiate the walls from the bottom and top surfaces. Several studies have shown that smooth muscle cells (SMCs) can produce a mesh of fibrous extracellular collagen during culture.[30–32] We hypothesized that collagen secretion would follow SMC cell density, which we could guide by introducing sharp corners and curvature in our micro-container design. **Figure 1** shows our strategy for developing micro-containers with preferential collagen coating along the side walls of the micro-containers. Niches were prepared using photopolymerizable methacrylated hyaluronic acid (MeHA) hydrogel following our previously reported protocols (Figure 1a).[33,34] The base area (4×10^4 μm^2) and the height (50 μm) of micro-containers were the same for all features used in this study. The inside of the micro-containers was coated with fibronectin to allow cell adhesion. SMCs were then seeded inside these micro-containers and the niches were closed with a hydrogel lid (Figure 1b). After culturing SMCs and collagen secretion, SMCs were removed by Ethylenediaminetetraacetic acid (EDTA) and Triton-X100 (Figure 1c), and then fibroblasts were seeded into the wells allowing us to study the influence of geometry on gap closure (Figure 1d,e).

First, we studied the distribution of collagen secreted by SMCs. SMCs were seeded in micro-containers with different geometries (cylindrical, cuboid, and prism), and allowed to spread and secrete extracellular collagen for 5 days. SMCs grew well in all geometries and exhibited similar well-developed F-actin filaments (**Figure 2**a). Collagen immunostaining showed that SMCs cultured in micro-containers produced fibrous collagen (Figure 2a). Notably, fibrous collagen derived from SMCs strongly accumulated around the edge and in the corner of micro-containers, while cells in the center secreted less, as shown by immunostaining and the collagen fluorescent intensity profile (Figure 2a). The SMCs were then removed by a previously described decellularization process,[35–37] which involved EDTA and Triton X100 treatment, followed by gently washing with phosphate buffered saline (PBS). As expected, after removal of cells, no nuclei could be observed, as confirmed by 4',6-diamidino-2-fenylindole (DAPI) staining, indicating that SMCs were fully removed from the micro-containers (Figure 2b). Fibronectin was washed away through this process (Figure S1, Supporting Information). Collagen was stained with anti-collagen I antibody, which showed insoluble collagen fibers present along the walls of the micro-containers, and only minimal amounts (fluorescence intensity barely above background level) of collagen on the bottom of the wells, as shown also by the collagen intensity profile in Figure 2b, which is consistent with previous studies in tissue decellularization.[38–40] The negative charges at the surface of MeHA may facilitate electrostatically driven adsorption of the positively charged collagen.[41] 3D images show homogenous distribution of secreted collagen on the sidewall of micro-containers, as shown in Figure 2c.

Next, we studied the apparent preference for collagen secretion by SMCs around the edges of the micro-containers. It has

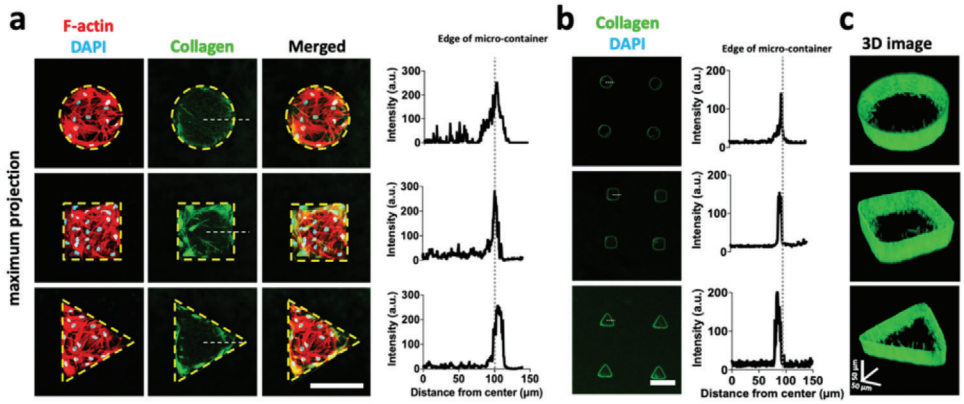

Figure 2. a) Immunofluorescent staining of F-actin, DAPI, and collagen for SMCs cultured in micro-containers with different geometries. Cells inside micro-containers with different geometries were fixed and stained after 5 days of culture. Scale bar is 200 μm. Line traces show collagen fluorescence intensity profiles of indicated white dashed lines from center to the edge of micro-container. b) Immunofluorescent images show DAPI and collagen staining in micro-containers after removal of SMCs. Scale bar is 400 μm. c) 3D constructed figures show collagen staining. The geometry of micro-container was indicated by yellow dashed lines. Line traces show collagen fluorescence intensity profiles from center to the edge of micro-container.

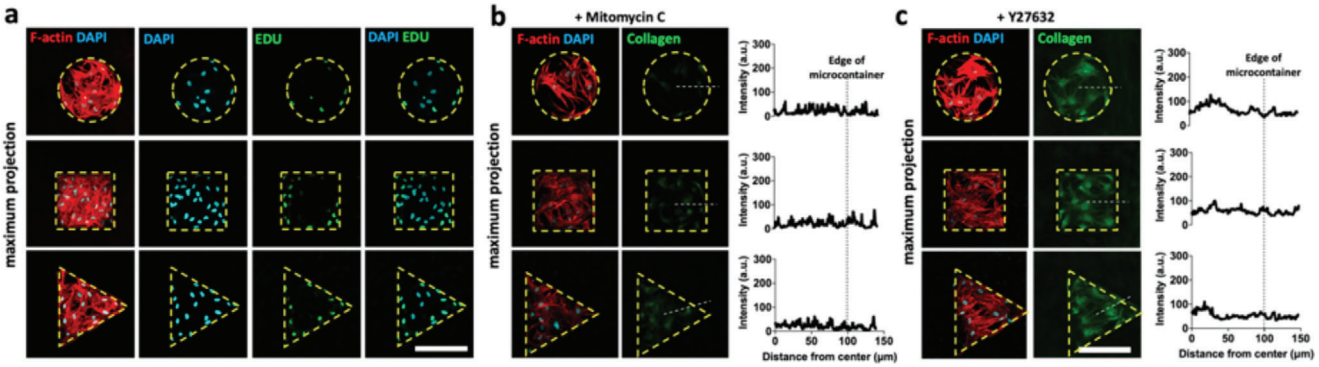

Figure 3. a) Immunofluorescent staining of F-actin, DAPI, and 5-ethynyl-2′-deoxyuridine (EDU) for SMCs cultured in micro-containers with different geometries. Merged images show colocalization of DAPI and EdU; proliferating cells are EdU positive in the images. b) Mitomycin C (10 μg mL^{-1}) to inhibit proliferation and c) Y-27632 (25 μM) to inhibit ROCK signaling. Scale bar is 200 μm for all figures. Line traces show collagen fluorescence intensity profiles of indicated white dashed lines from center to the edge of micro-container. The geometry of micro-container was indicated by dashed lines.

been reported that high cell proliferation rates coincide with higher collagen secretion by SMCs.[42] In line with this, we found more proliferating cells on the edges and corners of the micro-containers than in the center, as shown by 5-ethynyl-2´-deoxyuridine (EdU) staining (**Figure 3**a), which is also consistent with findings on flat cell sheets.[43] To address whether cell proliferation rate could direct secretion of collagen fibers in our micro-containers, we added mitomycin C (10 μg mL^{-1}) in the cell culture medium to inhibit cell proliferation,[44] which lowered collagen production by SMCs to an undetectable level (Figure 3b). In addition, decreasing contractile tension in cells by inhibiting Rho-kinases (ROCK) with Y-27632 (25 μM) also significantly reduced the collagen formation at the outer edge, resulting in a homogenous distribution of collagen staining inside the micro-containers (Figure 3c). Together, these findings indicate that cell proliferation and cytoskeletal tension induce SMCs to preferentially deposit a thin film of collagen in those areas where they proliferate most and develop highest contractile tension. This is along the edges of the micro-containers, and because the heights of the containers are not that high, both the edges and sidewalls of the micro-containers are the areas with preferential collagen deposits.

2.2. Gap Geometry Dictates Fibroblast Closure Efficiency

In order to create naturally formed gaps, fibroblasts were seeded in collagen-coated micro-containers at a very low density (≈20 cells/micro-container). We found that cells only adhered and spread along the edges and walls of micro-containers, irrespective of the size of the niche (**Figure 4**a and Figure S2a, Supporting Information). Cells seeded in micro-containers without any protein coating showed poor cell adhesion, whereas homogeneous collagen coatings (200 μg mL^{-1}) resulted in a random distribution of adhering cells (Figure S2b, Supporting Information). Cells in micro-containers homogeneously filled with collagen fibrillar hydrogel were randomly distributed and gradually filled the micro-containers (Figure S2c, Supporting Information). Thus, the localized collagen coating secreted by SMCs allowed us to produce an initial fibroblast distribution along the edges and

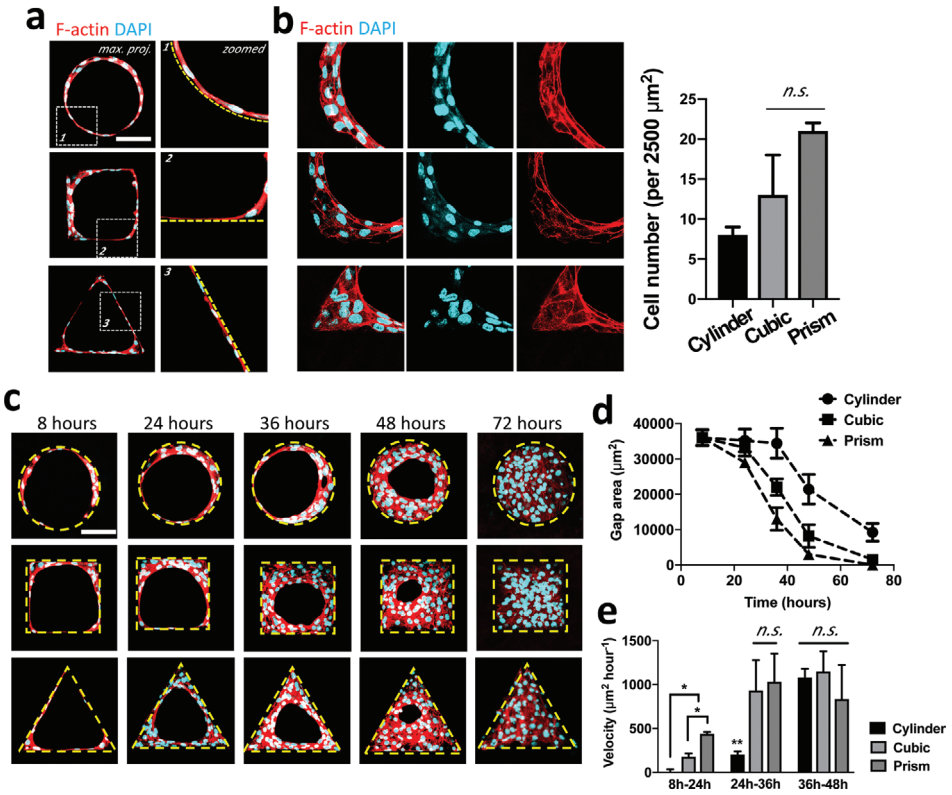

Figure 4. a) Immunofluorescent staining of F-actin and DAPI for fibroblasts cultured in micro-containers after removal of SMCs. Zoomed figures show the enlarged regions. b) F-actin and DAPI for fibroblasts with different angle sharpnesses at 8 h after seeding. Column figure shows quantification of cell density in micro-containers with different geometries. c) Representative images show F-actin and DAPI staining for fibroblasts during gap closure at different time points. d) Quantification of the gap area in micro-containers as a function of time. Data are reported as mean and SD of 30–40 gaps analyzed, resulting from three independent experiments. e) The bar graph shows the quantification of gap closure velocity in micro-containers with different geometries at different time ranges after cell seeding. $*p < 0.05$, $**p < 0.01$ indicating a significant difference between groups. n.s. = no significant difference; $n \geq 15$ regions of interest (ROI) with a total of 30–40 gaps analyzed. The geometry of micro-container was indicated by yellow dashed lines.

walls of the micro-containers, setting up well-defined starting geometries to study the rate of gap closure in such niches.

Cells only adhered to the edges and sides of the micro-containers, and closed the gap via collective migration toward the center. This presents an opportunity to study the role of geometrical factors in gap closure. Next, we analyzed how geometry affects the efficiency of gap closure. In all cases, we observed the elongation and alignment of F-actin and nuclei along the circumferential layer of cells. However, in the vertices of prism- and cuboid shaped, cell density was always higher compared to the walls of cylindrical shapes, and we did not observe distinct protrusions formed by cells in those micro-containers with different geometries, indicating a "purse-string" gap closure mechanism (Figure 4b). The closure of gaps started after cells were well-spread along the wall of the micro-containers. After 36 h of culture, the gaps formed an elliptical shape irrespective of starting geometry (Figure 4c). Among the three different geometries (where the starting area to be covered with cells was always 4×10^4 µm^2), we observed accelerated closing of gaps in the prism and cuboid micro-containers, compared to the cylindrical ones (Figure 4c,d; Figure S3, Supporting Information). However, this difference is primarily caused by a much longer "lag time" for cylindrical micro-containers, where the gap remains of more or less constant size for the first 40 h. Once gap closure was initiated, we found no significant differences for the different geometries (Figure 4e), indicating a common mechanism for gap closure.

2.3. Closure Is Driven by Cell Proliferation and Contractility

During the process of wound healing, cell proliferation is necessary to close the wound gap with matrix-producing fibroblasts.[7] Interestingly, we find that proliferation (as shown using an EdU assay) was more pronounced in geometries with sharp corners, with the percentage of proliferating cells in prism-shaped micro-containers around fourfold higher compared to cylindrical ones (**Figure 5**a). Tracing the position of proliferating cells, we found a clear correlation between the acuteness of the angles present in the micro-container and percentage of cells showing proliferation, as shown in Figure 5b. Higher densities of proliferating cells were always observed along the circumferential boundary of the wound edge in all geometries (Figure 5c).

Previous studies on planar cell sheets have proposed that two mechanisms can drive the closure of gaps.[2,7–9,16,22] The first one is "cell crawling," in which lamellipodia or filopodia protrusions play a key role. The second mechanism is called

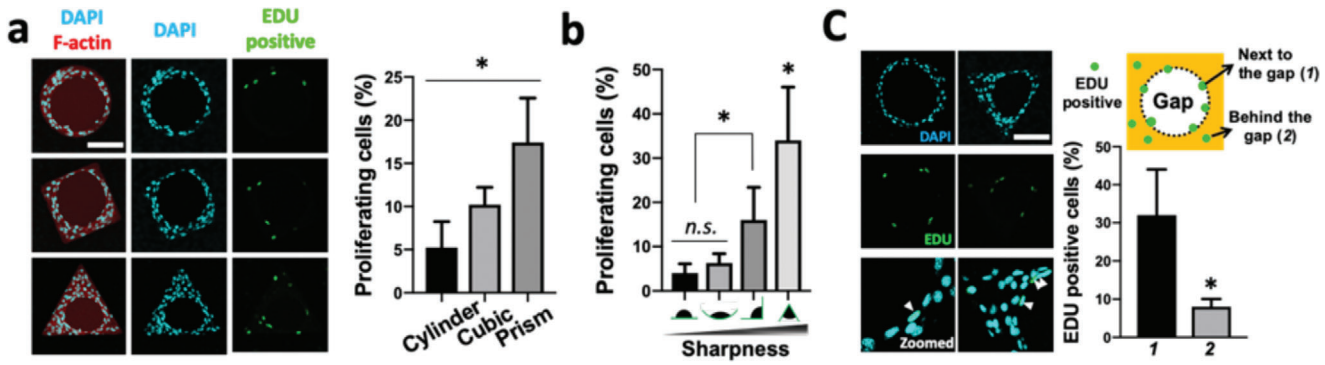

Figure 5. a) Immunofluorescent staining of F-actin, DAPI, and EdU for fibroblasts cultured in micro-containers with different geometries and percentage of proliferating cells in micro-containers with different geometries. b) Correlation between cell proliferation and sharpness of corners. c) Immunostaining images and quantification data show percentage of proliferating cells along the circumferential boundary of the wound edge and away from the wound edge. Scale bar is 100 μm in all figures. Data are presented as mean and SD of 12–18 gaps analyzed, resulting from three independent experiments. *$p < 0.05$ indicating a significant difference between groups. n.s. means no significant difference.

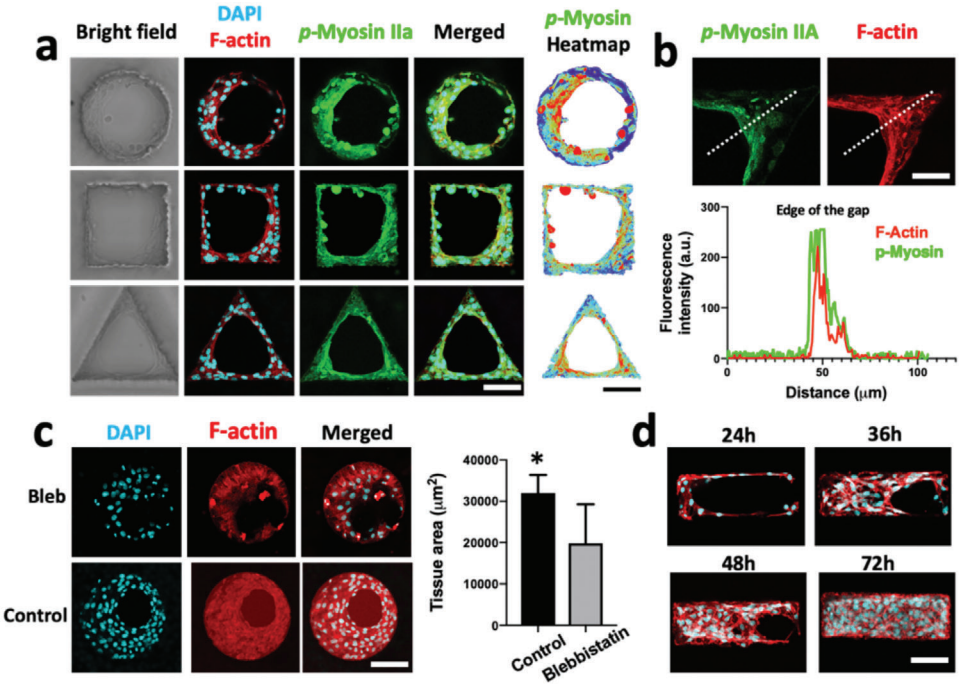

Figure 6. a) Immunofluorescent staining of F-actin, DAPI, and phospho-myosin IIa for fibroblasts cultured in micro-containers with different geometries. Heatmap shows the intensity of phospho-myosin IIa. Scale bar 100 μm. b) Top: Immunostaining figures show enlarged view of F-actin and phosphor-myosin IIa in sharp corner of prism micro-container. Bottom: Fluorescence intensity line profiles of the dashed lines. Scale bar 40 μm. c) Cells in micro-containers were treated with and without blebbistatin (50 μM) and stained with DAPI and F-actin. Histogram shows tissue area with and without blebbistatin treatment. Scale bar 100 μm. Data are presented as mean and SD of ≈ten gaps analyzed. *$p < 0.05$ indicating a significant difference between groups. d) Gap closure in cuboid shaped micro-container. Scale bar is 100 μm.

"purse-string" contraction, which involves the movement of all the cells along the edge due to the coordinated contraction of actin bundles and actomyosin cable. To investigate the role of actin and myosin during gap closure in this study, we stained cells with F-actin and *p*-myosin IIa. As shown in **Figure 6**a, no distinct protrusions were found in the cells along the edge of the gap. However, from the heatmap image of *p*-myosin, an actomyosin cable of high intensity could be clearly detected in cells surrounding the gap. The high intensity for *p*-myosin co-localized with the high intensity for F-actin (Figure 6b) provides some indication that the purse-string mechanism is involved, although we cannot clearly distinguish purse-strings that span multiple cells. We next examined whether actomyosin contractility affected gap closure. As expected, inhibition of non-muscle myosin II activity with blebbistatin significantly slowed down the closure rate (Figure 6c), indicating the critical role of cell-generated

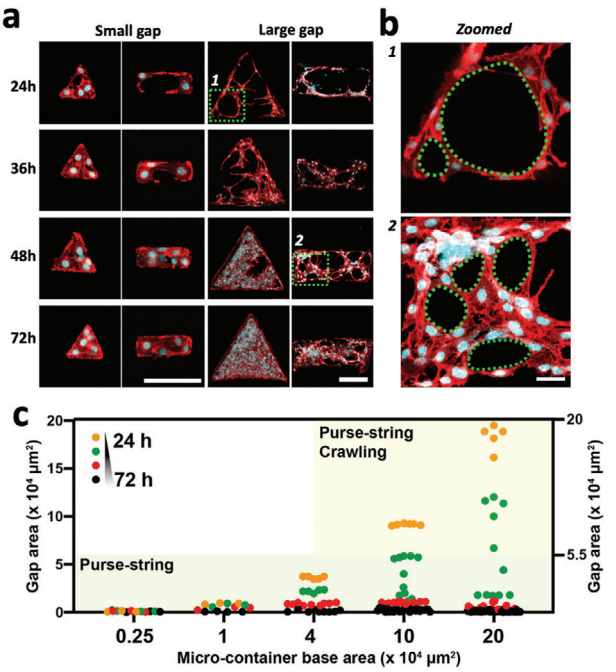

Figure 7. a) Immunofluorescent staining of F-actin (red) and DAPI (blue) for fibroblasts cultured in micro-containers with different sizes. The base area of the micro-container is 2500 μm^2 in the small gap, 100 000 μm^2 in the large gap. Scale is 100 μm. b) Zoomed figures show the enlarged regions in Figure 6a, indicated by green dash square. c) Quantification of the distribution of gap sizes in micro-containers with different base areas at different time points, and the related closure mechanism. Five to ten gaps analyzed for different conditions and different time points.

forces in gap closure, which is consistent with previous findings on flat substrates.[2] Changing the aspect ratio in the cuboid micro-containers yielded initial gaps with elongated shapes, which remained apparent during closure. These results indicate that the initial cell traction forces (from cells spreading along the corners of the micro-containers) play a key role in initiating the gap closure process (Figure 6d).

2.4. Gap Size Affects Gap Closure Mechanism

Previous studies on cell monolayers have shown that the size of gaps can cause the gap closure mechanism to switch between purse-string and cell crawling. In large gaps, closure is dominated by lamellipodium-mediated cell migration. In contrast, closure of smaller gaps proceeded by the purse-strong mechanism and exhibited the formation of actomyosin cables.[2,9] To test how gap size affects the gap closure mechanism in our systems, we designed micro-containers with different base areas (2500 and 100 000 μm^2). We did not observe any distinct protrusions and filopodia from cells seeded in 2500 μm^2 small gaps. However, in large gaps, protrusions and filopodia were clearly observed, as shown by F-actin staining in **Figure 7**a. Interestingly, we also observed smooth actin cables appearing during gap closure, indicating that cells adopted a combination of cell crawling and purse-string mechanism in large gaps (Figure 7b). In all micro-containers with large initial gaps, filopodia and cell crawling act to break up the large gap into smaller ones (indicated by green dashed lines in Figure 7b), which are then subsequently closed via a purse-string mechanism. From an analysis of the distribution of gap sizes formed, we estimate that the upper range of gap sizes still amenable for the purse-string mechanism is on the order of 55 000 μm^2. When the gap size in the range of ≈50 000 to 2 00 000 μm^2, we observed a combination of purse-string and cell crawling, where small gaps distributed in large gap were closed through purse-string. When the gap size is larger than 2 00 000 μm^2, only filopodia and protrusions were observed, indicating a cell-crawling closure mechanism (Figure 7c). In all micro-containers with large initial gaps, at the early stage of gap closure, cells closed the gap through crawling by forming lamellipodial protrusions. At later stages of gap closure, cells around the gap can collectively assemble a multi-cellular actomyosin bundle and close the gap through purse-string (Figure 7c).

3. Conclusion

In summary, the cell-guided protein patterning of micro-containers provides a robust method for patterned deposition of cells. We exploited this method to produce micro-containers filled with fibroblast in well-defined starting geometries, allowing us to study how cells closed the initial undamaged gaps present after seeding. We demonstrate that local geometry has a strong impact on gap closure rate, which can be explained by geometry-driven cell proliferation and contractility. We show that actin bundles and an actomyosin cable along the gap edge mediate cell migration to close small gaps, while cells adopt a combination of cell crawling and purse-string mechanism for large gaps. Although the contractility alignment of cells along the wound edge suggested that the fibroblasts adopted a purse string mechanism for gap closure, we do note that the presence of a multicellular actomyosin "purse-string" bundle is not prominent, and other closure mechanisms cannot be ruled out. The role of cell–ECM interactions during gap closure needs to be explored further. Furthermore, efficient formation and contraction of actin-based purse-strings might also be limited to cell types that are involved in wound healing (e.g., skin keratinocytes and embryonic epidermal cells), as simple epithelial cells such as Madin–Darby canine kidney cells are unable to close similar non-adhesive gaps efficiently. The geometry dependency observed here provides important new directions for future research in wound healing. The platform created in this study shows the importance of 3D patterning, and could spur new developments in 3D printing that could provide scaffolding materials with optimal microstructures to guide the rapid closure of wound gaps. An understanding of the effect of geometry on gap closure, pore filling, and tissue growth could help in the optimization of porous scaffolds for tissue engineering as well as improve understanding of the parameters that affect tissue remodeling and healing. In future studies, our studies can be expanded to include other cell types (including keratinocytes) and it will be important to investigate a range of other factors (including gel stiffness and porosity, fiber orientation, or gel deformation) and study how those factors can be coordinated with geometrical signals to affect gap closure.

4. Experimental Section

Fabrication of MeHA Micro-Containers with Different Geometries: MeHA micro-containers with different geometries were prepared according to the previously reported method.[33] Briefly, a silicon master with different geometries was fabricated by photolithography and inductively coupled plasma etching technique, then treated with 1H,1H,2H,2H-perfluordecyltriethoxysilane. A MeHA pre-hydrogel solution with photoinitiator lithium phenyl-2,4,6-trimethylbenzoylphosphinate was placed on top of the silicon master and exposed to UV light with a light output of 30% (UV lamp [ABM, USA] at 25 mW cm^{-2}) for 5 min to form the hydrogel with micro-containers. The surface of hydrogel was coated with PLL-g-PEG (SuSoS surface technology, 1 mg mL^{-1}) by placing the patterned surface of the gel on a polyacrylamide gel containing PLL-g-PEG. Fibronectin (100 µg mL^{-1}) was added on top of the gel to coat the micro-containers. After seeding cells in micro-containers, a permeable MeHA hydrogel with fibronectin coating was used as a lid to create a closed micro-container and prevent cells from migrating outside of the micro-containers.

Fabrication of MeHA Micro-Containers with Deposited Collagen by SMCs: SMCs from mouse can secrete high levels of collagen under basal conditions and were used at passage 6–10 for all experiments in this study. SMCs were grown in Dulbecco's modified Eagle's medium (DMEM) supplemented with 10% FBS, 1% L-glutamine, and 1% Pen/Strep (Thermo fisher scientific). SMCs were trypsinized with 0.05% trypsin/EDTA until reaching 80% confluence and then seeded in the MeHA micro-containers at a density of 20 000 cells cm^{-2}. SMCs were cultured in micro-containers for 5 days for proliferation and secretion of collagen, and then removed by sequentially treating with 0.05% EDTA and 0.1% Triton X-100 for 5 min (the time can be extended if cells are not fully detached from the micro-containers). Gentle washing with PBS (3×) washed away remaining fibronectin, and the resulting micro-containers were then aseptically dried in a laminar air flow cell culture for later use.

NIH3T3 Fibroblast Culture and Seeding: NIH 3T3 cells were cultured in DMEM medium with high glucose (4.5 g L^{-1}) containing 10% FBS and 1% Pen/Strep; cells were trypsinized and seeded in micro-containers with deposited collagen at a density of 5000 cells cm^{-2}, resulting in ×20 cells/micro-container. After seeding, cells were incubated for 10–15 min and then the MeHA hydrogel was gently washed with culture medium to remove non-adherent cells, and a hydrogel lid was placed on top subsequently.

Inhibitor Experiments: The inhibitor experiments were performed by adding different inhibitors into the cell culture medium. To inhibit proliferation of SMCs, mitomycin C (10 µg mL^{-1}; Sigma) was added to cell culture medium for 2 h and washed three times with media. Y-27632 (25 µM, Sigma) was added to cell culture medium for 2 h to inhibit ROCK signaling. Myosin II activity was inhibited by treating cells with blebbistatin (50 µM, Sigma) for 1 h.

Immunostaining: For immunostaining, cells were fixed with 4% paraformaldehyde (Sigma) for 10 min at room temperature. The hydrogel lid was gently removed after fixation; the cells were permeabilized with 0.1% Triton X-100 for 10 min, followed by washing thrice with PBS and blocked with 1% BSA in PBS for 1 h. Then, cells were incubated with different primary antibodies against phospho-myosin light chain 2 (Thr19/Ser19) (Cell Signalling Technologies, 3674, 1:100), collagen I (Abcam, ab34710, 1:100) overnight at 4 °C, and detected with goat anti-rabbit Alexa 488 (1:500)-conjugated secondary antibodies. Cell nuclei and actin cytoskeleton were stained with DAPI (Millipore, 1:1000 in 1% BSA) and phalloidin tetramethyl-rhodamine B isothiocyanate (Millipore, R415, 1:1000 in 1% BSA). Fluorescent images were obtained using a Leica SP8 inverted confocal microscope.

Cell Proliferation Assay: EdU labeling was performed to examine cell proliferation as the previous report.[45] Fibroblasts were seeded in micro-containers for 8 h and then treated with 1 × EdU solution. After 24 h of culture, cells were fixed and sequentially treated with 4% PFA and 0.1% Triton X-100, respectively. Afterward, samples were stained according to the manufacturer's protocol of Click-iT EdU Alexa Fluor-488 HCS Assay (Thermo Fisher Scientific). All images were collected by a Leica SP8 confocal microscope (Leica, Germany) with filters for DAPI and Alexa Fluor-488. Cells showed that positive EDU staining was quantified as proliferating cells.

Image Analysis: All images were taken with different z-stacks by using a Leica SP8 confocal microscope. Images with different z-stacks were then overlaid in Fiji software with Image 5D plugin to get the maximum projection view. 3D reconstructions of staining images were generated in Leica LASX Software. Collagen intensity measurements were performed by using line-profile function in Fiji software. All images used for intensity quantification were taken under the photon counting mode.

Statistics: In Figure 4D,E, $n \geq 15$ regions of interest with a total of 30–40 gaps were analyzed in four different experiments. In Figure 5, 12–18 gaps were analyzed from three independent experiments. In Figure 6C, approximately ten gaps were analyzed. In Figure 7, five to ten gaps were analyzed from at least three independent experiments for different conditions and different time points. Data analysis, statistics, and graph plotting were performed using Prism (GraphPad) software. Statistical analysis was performed by one-way analysis of variance (ANOVA) test. *p*-Values less than 0.05 were considered statistically significant.

Supporting Information

Supporting Information is available from the Wiley Online Library or from the author.

Acknowledgements

M.B. and J.X. contributed equally to this work. The authors are grateful to the Department of General Instruments of the Radboud University for providing confocal and light microscopy services. The authors acknowledge financial support from the China Scholarship Council (J.X. and X.H.).

Conflict of Interest

The authors declare no conflict of interest.

Keywords

hydrogels, wound healing, cell spreading, microniches

Received: April 17, 2020
Revised: June 26, 2020
Published online: August 6, 2020

[1] G. C. Gurtner, S. Werner, Y. Barrandon, M. T. Longaker, *Nature* **2008**, *453*, 314.
[2] A. Ravasio, I. Cheddadi, T. Chen, T. Pereira, H. T. Ong, C. Bertocchi, A. Brugues, A. Jacinto, A. J. Kabla, Y. Toyama, *Nat. Commun.* **2015**, *6*, 7683.
[3] S. Begnaud, T. Chen, D. Delacour, R.-M. Mège, B. Ladoux, *Curr. Opi. Cell Biol.* **2016**, *42*, 52.
[4] E. Marinari, A. Mehonic, S. Curran, J. Gale, T. Duke, B. Baum, *Nature* **2012**, *484*, 542.
[5] P. Martin, *Science* **1997**, *276*, 75.
[6] E. Brauer, E. Lippens, O. Klein, G. Nebrich, S. Schreivogel, G. Korus, G. N. Duda, A. Petersen, *Adv. Sci.* **2019**, *6*, 1801780.
[7] M. S. Sakar, J. Eyckmans, R. Pieters, D. Eberli, B. J. Nelson, C. S. Chen, *Nat. Commun.* **2016**, *7*, 11036.

[8] S. R. K. Vedula, G. Peyret, I. Cheddadi, T. Chen, A. Brugués, H. Hirata, H. Lopez-Menendez, Y. Toyama, L. N. De Almeida, X. Trepat, *Nat. Commun.* **2015**, *6*, 6111.
[9] E. Anon, X. Serra-Picamal, P. Hersen, N. C. Gauthier, M. P. Sheetz, X. Trepat, B. Ladoux, *Proc. Natl. Acad. Sci. USA* **2012**, *109*, 10891.
[10] M. S. Sakar, J. Eyckmans, R. Pieters, D. Eberli, B. J. Nelson, C. S. Chen, *Nat. Commun.* **2016**, *7*, 11036.
[11] R. Farooqui, G. Fenteany, *J. Cell Sci.* **2005**, *118*, 51.
[12] M. Tamada, T. D. Perez, W. J. Nelson, M. P. Sheetz, *J. Cell Biol.* **2007**, *176*, 27.
[13] P. Martin, J. Lewis, *Nature* **1992**, *360*, 179.
[14] G. Fenteany, P. A. Janmey, T. P. Stossel, *Curr. Biol.* **2000**, *10*, 831.
[15] M. T. Abreu-Blanco, J. M. Verboon, R. Liu, J. J. Watts, S. M. Parkhurst, *J. Cell Sci.* **2012**, *125*, 5984.
[16] M. Poujade, E. Grasland-Mongrain, A. Hertzog, J. Jouanneau, P. Chavrier, B. Ladoux, A. Buguin, P. Silberzan, *Proc. Natl. Acad. Sci. USA* **2007**, *104*, 15988.
[17] A. A. Khalil, P. Friedl, *Integr. Biol.* **2010**, *2*, 568.
[18] W. M. Bement, P. Forscher, M. S. Mooseker, *J. Cell Biol.* **1993**, *121*, 565.
[19] A. Jacinto, A. Martinez-Arias, P. Martin, *Nat. Cell Biol.* **2001**, *3*, E117.
[20] Y. Matsubayashi, M. Ebisuya, S. Honjoh, E. Nishida, *Curr. Biol.* **2004**, *14*, 731.
[21] B. Hu, W. R. Leow, S. Amini, B. Nai, X. Zhang, Z. Liu, P. Cai, Z. Li, Y. L. Wu, A. Miserez, *Adv. Mater.* **2017**, *29*, 1700145.
[22] A. Brugués, E. Anon, V. Conte, J. H. Veldhuis, M. Gupta, J. Colombelli, J. J. Muñoz, G. W. Brodland, B. Ladoux, X. Trepat, *Nat. Phys.* **2014**, *10*, 683.
[23] V. Nier, M. Deforet, G. Duclos, H. G. Yevick, O. Cochet-Escartin, P. Marcq, P. Silberzan, *Proc. Natl. Acad. Sci. USA* **2015**, *112*, 9546.
[24] M. Bao, J. Xie, W. T. Huck, *Adv. Sci. 5*, **2018**, 1800448.
[25] S. R. K. Vedula, M. C. Leong, T. L. Lai, P. Hersen, A. J. Kabla, C. T. Lim, B. Ladoux, *Proc. Natl. Acad. Sci. USA* **2012**, *109*, 12974.
[26] C.-C. Liang, A. Y. Park, J.-L. Guan, *Nat. Protoc.* **2007**, *2*, 329.
[27] C. R. Keese, J. Wegener, S. R. Walker, I. Giaever, *Proc. Natl. Acad. Sci. USA* **2004**, *101*, 1554.
[28] S. J. Hollister, *Nat. Mater.* **2005**, *4*, 518.
[29] P. Kollmannsberger, C. M. Bidan, J. W. Dunlop, P. Fratzl, V. Vogel, *Sci. Adv.* **2018**, *4*, eaao4881.
[30] M. F. Graham, D. E. Drucker, R. F. Diegelmann, C. O. Elson, *Gastroenterology* **1987**, *92*, 400.
[31] S. A. Hurd, N. M. Bhatti, A. M. Walker, B. M. Kasukonis, J. C. J. B. Wolchok, *Biomaterials* **2015**, *49*, 9.
[32] P. A. Jones, T. Scott-Burden, W. Gevers, *Proc. Natl. Acad. Sci. USA* **1979**, *76*, 353.
[33] M. Bao, J. Xie, A. Piruska, W. T. Huck, *Nat. Commun.* **2017**, *8*, 1962.
[34] M. Bao, J. Xie, N. Katoele, X. Hu, B. Wang, A. Piruska, W. T. Huck, *ACS Appl. Mater. Interfaces* **2019**, *11*, 1754.
[35] J. Zhou, O. Fritze, M. Schleicher, H.-P. Wendel, K. Schenke-Layland, C. Harasztosi, S. Hu, U. A. Stock, *Biomaterials* **2010**, *31*, 2549.
[36] P. M. Crapo, T. W. Gilbert, S. F. Badylak, *Biomaterials* **2011**, *32*, 3233.
[37] G. Gao, J. H. Lee, J. Jang, D. H. Lee, J. S. Kong, B. S. Kim, Y. J. Choi, W. B. Jang, Y. J. Hong, S. M. Kwon, *Adv. Funct. Mater.* **2017**, *27*, 1700798.
[38] Q. Xing, C. Vogt, K. W. Leong, F. Zhao, *Adv. Funct. Mater.* **2014**, *24*, 3027.
[39] X. Tian, M. E. Werner, K. C. Roche, A. D. Hanson, H. P. Foote, K. Y. Stephanie, S. B. Warner, J. A. Copp, H. Lara, E. L. Wauthier, *Nat. Biomed. Eng.* **2018**, *2*, 443.
[40] R. Edri, I. Gal, N. Noor, T. Harel, S. Fleischer, N. Adadi, O. Green, D. Shabat, L. Heller, A. Shapira, *Adv. Mater.* **2019**, *31*, 1803895.
[41] S. Chen, Q. Zhang, T. Nakamoto, N. Kawazoe, G. Chen, *J. Mater. Chem. B* **2014**, *2*, 5612.
[42] J. M. Burke, R. Ross, *Exp. Cell Res.* **1977**, *107*, 387.
[43] C. M. Nelson, R. P. Jean, J. L. Tan, W. F. Liu, N. J. Sniadecki, A. A. Spector, C. S. Chen, *Proc. Natl. Acad. Sci. USA* **2005**, *102*, 11594.
[44] R. McBeath, D. M. Pirone, C. M. Nelson, K. Bhadriraju, C. S. Chen, *Dev. Cell* **2004**, *6*, 483.
[45] J. Xie, M. Bao, S. p. M. Bruekers, W. T. Huck, *ACS Appl. Mater. Interfaces* **2017**, *9*, 19630.